Diffractive optics for quasi-direct space-to-time pulse shaping

Gladys Mínguez-Vega,[1,*] Omel Mendoza-Yero,[1] Jesús Lancis,[1] Rafael Gisbert,[1] and Pedro Andrés[2]

[1] *GROC, Departament de Física, Universitat Jaume I, 12080 Castelló, Spain.*
[2] *Departament d'Òptica, Universitat de València, 46100 Burjassot, Spain.*
[*] *Corresponding author: gminguez@uji.es*

Abstract: The strong chromatic behavior associated with a conventional diffractive lens is fully exploited to propose a novel optical device for pulse shaping in the femtosecond regime. This device consists of two optical elements: a spatially patterned circularly symmetric mask and a kinoform diffractive lens, which are facing each other. The system performs a mapping between the spatial position of the masking function expressed in the squared radial coordinate and the temporal position in the output waveform. This space-to-time conversion occurs at the chromatic focus of the diffractive lens, and makes it possible to tailor the output central wavelength along the axial location of the output point. Inspection of the validity of our device is performed by means of computer simulations involving the generation of femtosecond optical packets.

OCIS codes: (050.1965) Diffractive lenses; (320.5540) Pulse shaping.

References and links

1. J. Capmany and D. Novak, "Microwave photonics combines two worlds," Nat. Photonics **1**, 319-330 (2007).
2. A. M. Weiner, "Femtosecond pulse shaping with spatial light modulators," Rev. Sci. Instrum. **71**, 1929-1960 (2000).
3. A. Assion, T. Baurmert, M. Bergt, B. Kiefer, V. Seyfried, M. Strehle, and G. Gerber, "Control of chemical reactions by feedback-optimized phase-shaped femtosecond laser pulses," Science **282**, 919-922 (1998).
4. C. Nuss and R. L. Morrison, "Time-domain images," Opt. Lett. **20**, 740-742, (1995).
5. D. M. Marom, D. Panasenko, P.-C. Sun, and Y. Fainman, "Spatial-temporal wave mixing for space-to-time conversion," Opt. Lett. **24**, 563-565 (1999).
6. C. Froehly, B. Colombeau, and M. Vampouille, "Shaping and analysis of picosecond light pulses," in *Prog. Opt. XX*, E. Wolf, ed., 65–153 (North-Holland, Amsterdam, 1983).
7. D. E. Leaird and A. M. Weiner, "Femtosecond optical packet generation by a direct space-to-time pulse shaper," Opt. Lett. **24**, 853-855 (1999).
8. J. D. McKinney, D. E. Leaird, and A. M. Weiner, "Millimiter-wave arbitrary waveform generation with a direct space-to-time pulse shaper," Opt. Lett. **27**, 1345-1347 (2002).
9. S. Xiao, J. D. McKinney, and A. M. Weiner, "Photonic microwave arbitrary waveform generation using a virtual imaged phased-array direct space-to-time pulse shaper," IEEE Photon. Technol. Lett. **16**, 1936-1938 (2004).
10. V. Moreno, J. F. Roman, and J. R. Salgueiro, "High efficiency diffractive lenses: Deduction of kinoform profile," Am. J. Phys. **65**, 556-562 (1997).
11. Y. X. Wang, W. B. Yun, and C. Jacobsen, "Achromatic Fresnel optics for wideband extreme-ultraviolet and X-ray imaging," Nature **424**, 50-53 (2003).
12. M. Hacker, G. Stobrawa, R. Sauerbrey, T. Buckup, M. Motzkus, M. Wildenhain, and A. Gehner, "Micromirror SLM for femtosecond pulse shaping in the ultraviolet," Appl. Phys. B **76**, 711-714 (2003).
13. B. J. Pearson and T. C. Weinacht "Shaped ultrafast laser pulses in the deep ultraviolet," Opt. Express **15**, 4385-4388 (2007). http://www.opticsinfobase.org/abstract.cfm?URI=oe-15-7-4385.
14. See, for instance, about Linac Coherent Light Source at http://lcls.slac.stanford.edu/.
15. A. G. Michette, *Optical Systems for Soft X-Rays* (Plenum, 1986).
16. Z. Bor, "Distortion of femtosecond laser pulses in lenses," Opt. Lett. **14**, 119-121 (1989).
17. G. Mínguez-Vega, O. Mendoza-Yero, J. Lancis, and V. Climent, "Proposal for the generation of THz bursts and codes of shaped femtosecond pulses using binary mask," IEEE Photon. Technol. Lett. **19**, 1732-1734 (2007).
18. C. G. Leburn, A. A. Lagatsky, C. T. A. Brown and W. Sibbett, "Femtosecond Cr^{4+}:YAG laser with 4 GHz pulse repetition rate," Electron. Lett. **40**, 805-807 (2004).

#98973 - $15.00 USD Received 18 Jul 2008; revised 22 Sep 2008; accepted 23 Sep 2008; published 10 Oct 2008

1. Introduction

Photonic processing of telecom signals is a research topic that has been explored for more than 30 years [1] and the use of pulse-shaping technology has been acknowledged [2] as a convenient framework for synthesizing user-defined temporal waveforms. As an example, photonic generation of pulse trains with a repetition rate in the terahertz scale is relevant to support the requirements of high-bit-rate transmission. Both coherent and spectrally incoherent optical sources have been employed. Although incoherent processing is usually preferred for microwave signal filtering owing to the greater signal stability achieved, the use of a coherent source allows for both intensity and phase shaping, which is relevant, for instance, in quantum control [3].

Pulse shaping is usually performed through a space-to-time transformation, where spatial masking of an optical beam causes its temporal modulation. In the Fourier-transform pulse-shaping technique, the conversion is achieved by spectrum equalization through complex amplitude modulation on the Fourier plane of a zero-dispersion grating device. Usually spatial light modulators (SLM), such as a liquid crystal SLM or an acoustic-optic modulator, substitute the fixed mask to achieve a programmable pulse shaping [2]. More sophisticated pulse processing operations have been used to convert spatial-domain images to ultrafast time-domain optical waveforms with fixed computer-generated holograms [4] or dynamic real-time holographic material in a four-wave mixing arrangement [5].

Although initially implemented for input pulses in the picosecond time scale [6], the so-called direct space-to-time (DST) pulse shaper has been adapted to the femtosecond range and promoted as a fast data encoder [7]. The idea is that the spatial mask itself acts as the temporal filter, in contrast to the behavior of a Fourier pulse shaper, where a Fourier transform operation is required for the design of the temporal filter. This reduces the computation time and thus allows for faster operation. The three building blocks of the DST pulse shaper are: 1) spatial masking that can be programmable by using a SLM; 2) wavelength dispersion either through a diffraction grating [8] or even with a virtually-imaged phased array for higher resolution [9]; and 3) beam focusing through a chromatically corrected refractive objective.

In this manuscript, we describe a quasi-direct space-to-time (QDST) pulse shaper consisting of a mask attached to a kinoform diffractive lens (DL) [10]. The term quasi-direct refers to a space-to-time transformation from the squared radial coordinate to time. Unlike the DST pulse shaper, in our system beam dispersion and focusing are performed exclusively in terms of diffraction. This inherent diffractive nature grants a pulse-shaping device new functionality and flexibility, namely: 1) The mask function and the DL can be implemented together in a single SLM, thereby providing an easy-to-align, compact real-time pulse shaper; and 2) It is suitable for controlling and manipulating beams in the extreme ultraviolet (XUV) or x-ray spectral region, where refractive lenses cannot be used due to the absorption of materials. Fresnel zone plates (the less efficient version of the DL) have already been successfully applied in these regions of the electromagnetic spectrum [11]. The availability of shaped pulses in the UV can be applied in the control of electronic responses of atoms and molecules. In this region, micro-mirror SLM and acousto-optic devices are now employed in a Fourier pulse-shaping geometry [12,13]. Moreover, femtosecond pulses from a hard x-ray free-electron laser, which will open up new horizons for femtochemistry, nanoscale dynamics and molecular biological science, are currently under construction [14].

2. All-diffractive pulse shaper device

Figure 1 shows a schematic representation of the QDST pulse shaper. A pulsed plane-wave emitted by a femtosecond laser oscillator with a carrier frequency of ω_0 is used to illuminate the system. The temporal amplitude associated with the input pulse is denoted by $u_{in}(t)$. The optical device is made up of a circularly symmetric mask with complex transmittance $t(r)$ attached to a DL. The DL has a focal length of $Z(\omega) = Z_0 \omega / \omega_0$, where Z_0 is the focal length for ω_0. The output point is located at the axial distance z from the composed elements, where

#98973 - $15.00 USD Received 18 Jul 2008; revised 22 Sep 2008; accepted 23 Sep 2008; published 10 Oct 2008

a pinhole gathers the diffracted light. To ensure high efficiency we limit the *z* position to the focal range of the DL. For our mathematical treatment $z = Z(\omega_1)$ is considered, being ω_1 a spectral component of the incident pulse spectrum.

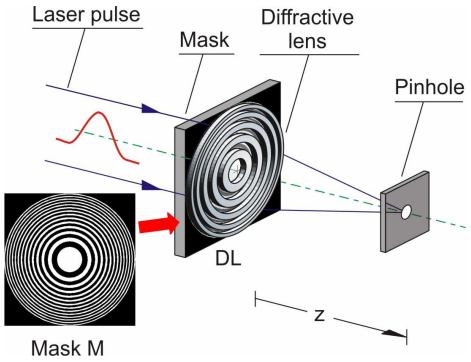

Fig. 1. Schematic diagram of the all-diffractive pulse shaper.

In order to study the propagation of an ultrafast pulse through the pulse-shaper device, we first consider one spectral component of frequency ω within the amplitude spectrum of the incident pulse, $\tilde{S}(\tilde{\omega})$, where $\tilde{\omega} = \omega - \omega_0$. Here, $\tilde{S}(\tilde{\omega})$ is the Fourier transform of $u_{in}(t)$. The on-axis amplitude distribution $\tilde{U}_{out}(\omega)$ at the output point is assessed by means of the generalized Huygens-Fresnel diffraction integral expressed in terms of the ABCD matrix for a cylindrical coordinate system

$$\tilde{U}_{out}(\omega) = \frac{\omega}{iBc}\tilde{S}(\tilde{\omega})exp\left[i\frac{\omega}{c}L\right]\int_o^\infty t(r)exp\left[i\frac{\omega}{c}\frac{A}{2B}r^2\right]rdr \quad . \qquad (1)$$

In Eq. (1), L is the on-axis optical path length between the input and output planes, which coincides with $Z(\omega_1)$ in the proposed system. To determine the values of elements *A* and *B*, the *ABCD* matrices associated with the DL and with the free-space propagation through the length $Z(\omega_1)$ are multiplied as follows

$$\begin{pmatrix} A & B \\ C & D \end{pmatrix} = \begin{pmatrix} 1 & Z_0\omega_1/\omega_0 \\ 0 & 1 \end{pmatrix}\begin{pmatrix} 1 & 0 \\ -\omega_0/Z_0\,\omega & 1 \end{pmatrix}. \qquad (2)$$

Note that the thin lens approximation for the DL used in this mathematical formalism holds whenever its number of periods is more than 100 [15]. For our purposes it is convenient to express the complex transmittance of the mask $t(r)$ as a function of a new variable, defined as $\mu = r^2$ in such a way that $q(\mu) = t(r)$. Here phase and amplitude information can be stored in the function $q(\mu)$. The output field can now be expressed as

$$\tilde{U}_{out}(\omega) = \frac{\omega}{i2Z(\omega_1)c}exp\left[i\frac{\omega}{c}Z(\omega_1)\right]\tilde{S}(\tilde{\omega})\tilde{Q}\left[\frac{\omega-\omega_1}{2cZ(\omega_1)}\right] \quad , \qquad (3)$$

where $\tilde{Q}$ is the spatial Fourier transform of $q(\mu)$. The ω in front of the exponential function can be approximated by ω_0 with a negligible error for pulse durations longer than 10 fs. Then, the output temporal amplitude $u_{out}(t)$ given by the inverse Fourier transform of Eq. (3) yields

#98973 - $15.00 USD Received 18 Jul 2008; revised 22 Sep 2008; accepted 23 Sep 2008; published 10 Oct 2008

$$u_{out}(\tau) = -i\omega_0\, u_{in}(\tau) \otimes \left[q\left(\frac{\tau}{\beta}\right) exp\left(-i\omega_1 \tau\right) \right] \quad , \tag{4}$$

where the symbol $\otimes$ stands for the convolution operation and $\tau = t - Z(\omega_1)/c$ is the proper time. The QDST conversion constant, which gives the mapping from the radial square spatial coordinate of the input mask to the temporal duration at the pulse shaper output, is provided by $\beta = 1/\left(2cZ(\omega_1)\right)$. The value of β coincides with the propagation time difference (PTD) per millimeter square between the phase and pulse fronts along the cross-section of the DL. This PTD can be calculated by geometrical arguments, as stated in [16].

Equation (4) is the main analytical result of this paper. It shows that the synthesized waveform is a convolution of the input ultrashort pulse with a scaled representation of the function $q(\mu)$ (whose spatial dependence has been converted into a temporal one characterized by the scale factor β) multiplied by a linear phase term that represents a frequency shift. Control of the output temporal waveform by constructing the appropriate mask can be a valuable technique when production of such waveforms by other methods is impossible or complicated. Note that when the time width of the input temporal amplitude is much shorter than the minimum feature size of the temporally mapped mask, $u_{in}(t)$ can be approximated by a Dirac function, and the output temporal amplitude is mainly the function $q(\tau/\beta)$. When this approximation does not hold, the output waveform is a smoothed version of $q(\tau/\beta)$ due to the convolution operation.

3. Numerical simulations

To corroborate the goodness of the mathematical treatment, we perform some numerical simulations by direct application of Eq. (1). Specifically, we illustrate the use of the QDST pulse shaper for the generation of a train of *N* identical equally-space flat-topped pulses. To this end, the mask is made up of a set of *N* annular apertures with the same areas. It is periodic in the squared radial coordinate, with a period given by p^2. The inner and outer radii of the rings fulfill the conditions $r_{im} = p\sqrt{m}$ and $r_{om} = p\sqrt{m+\varepsilon}$, where $0 < \varepsilon < 1$ and $m = 0,1,2,...N-1$. These masks were recently proposed for the generation of THz bursts of pulses for telecommunications [17]. Observe that in the optical system of [17] there is no DL to focus the light, so the output pulses are obtained from the superposition of the 2N boundary wave pulses emitted from the edges of the annular apertures. In contrast, the QDST pulse shaper uses the mask to tailor the PTD caused by the DL. This leads to an efficiency several orders of magnitude bigger and a higher degree of versatility in the pulse design.

For simulation purposes, the pulsed radiation emitted by a Cr^{+4}:YAG laser is used [18]. Its center wavelength is of $\lambda_0 = 1525$ nm and the standard deviation width of the Gaussian temporal instantaneous intensity yields 41.7 fs. The mask has realistic values of p = 5.5 mm, ε = 0.5, $N = 14$, and a maximum diameter of about 4 cm. The width of the narrowest ring in the mask is of 0.4 mm so it can be fabricated with conventional lithography techniques by using direct laser writing on a chrome photomask. This mask is depicted in Fig. 1 and from now on it will be referred to as mask M. The focal length of the DL is Z_0 = 100 mm. When the pinhole is located at the above focal position β = 16.6 fs/mm^2. The instantaneous intensity profiles obtained at z = 98 mm, z = 100 mm and z = 102 mm are plotted together in Fig. 2(a). They correspond to a sequence of pulses with a frequency of 1.98 THz. The different plots are superimposed, which indicates that the output signal is unaffected by the change of z when we move along the focal region of the DL. In this range, the change in the value of β is negligible. However, variations in the z position of the pinhole change the center wavelength

#98973 - $15.00 USD Received 18 Jul 2008; revised 22 Sep 2008; accepted 23 Sep 2008; published 10 Oct 2008

of the pulses (shift effect). For z = 100 mm, the output spectrum in logarithm scale is plotted as an inset in Fig. 2(b). This figure also shows the normalized power spectrum for z = 98 mm (short-dashed line), z = 100 mm (continuous line) and z = 102 mm (long-dashed line). The spectrum shift can be clearly appreciated by inspecting the position of the peaks. For each z distance the central wavelength takes the values of 1555 nm, 1525 nm and 1494 nm, respectively.

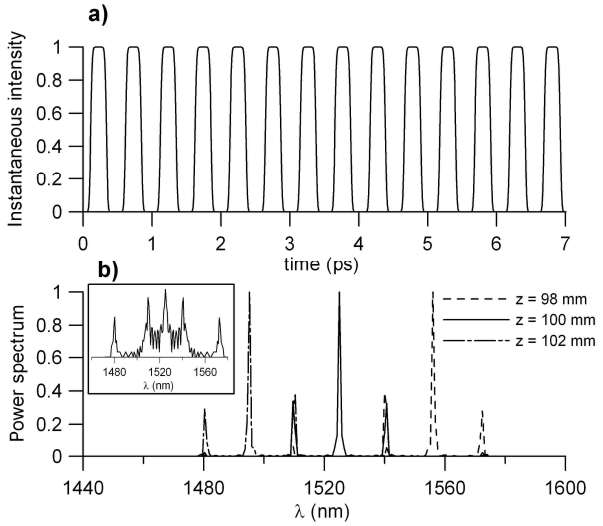

Fig. 2. Temporal and spectral response of the system plotted in Fig. 1. (a) Normalized instantaneous intensity, and (b) Normalized power spectrum. In both cases, three different z distances were considered: z = 98 mm (short-dashed curve), z = 100 mm (solid curve) and z = 102 mm (long-dashed curve). For z = 100 mm, the power spectrum in logarithmic scale is shown as an inset.

Next, we explain the spatiotemporal distribution in the output plane of the QDST pulse shaper, which was used to generate a data code pattern. Binary code patterns are crucial as optical packet-headers in packet-switched networks and for the photonically-assisted generation of microwave and millimeter-wave arbitrary waveforms [8,9]. The mask that was employed is shown in Fig. 3(a) and we call it mask N. It has the same characteristics as mask M but some rings have been removed. Figure 3(b) shows the output spatiotemporal intensity distribution calculated for the above system parameters at z = 100 mm. This is carried out numerically by solving the Huygens-Fresnel diffraction integral. A sequence of pulses with the same temporal duration is observed. We note that to obtain equal-amplitude pulses a small pinhole is required. For clarity, in Fig. 3(c) we show the instantaneous intensity for two pinhole sizes, with radii of r = 0.5 μm and r = 40 μm, integrated over the whole area of the pinhole. To mitigate the reduction of the amplitude arising from the finite pinhole radius, the amplitude of the output pulses can be modulated to have equal values by truncating the rings of the mask. To illustrate the effect of a transversal mismatch of the pinhole position, the instantaneous intensity for a 2 μm off-center punctual pinhole is also shown in Fig. 3(c). These effects that are imposed by experimental/construction parameters are subjects for continuing study.

Finally, we consider the efficiency of the QDST pulse shaper. A simple calculation of the efficiency can be performed by integrating the output power relative to the input power for the carrier frequency. Although the simulation does not consider losses due to the diffraction efficiency of a real DL, it is useful as an upper limit to the available output power. Figure 3 (d) shows the resulting efficiency calculated in terms of the pinhole size, for the masks and parameters used in the previous simulations and at z = 100 mm. With our system parameters,

#98973 - $15.00 USD Received 18 Jul 2008; revised 22 Sep 2008; accepted 23 Sep 2008; published 10 Oct 2008

the efficiency increases linearly as the pinhole radius increases until it reaches approximately 35 μm. Beyond this point, the increase of the efficiency is very slow.

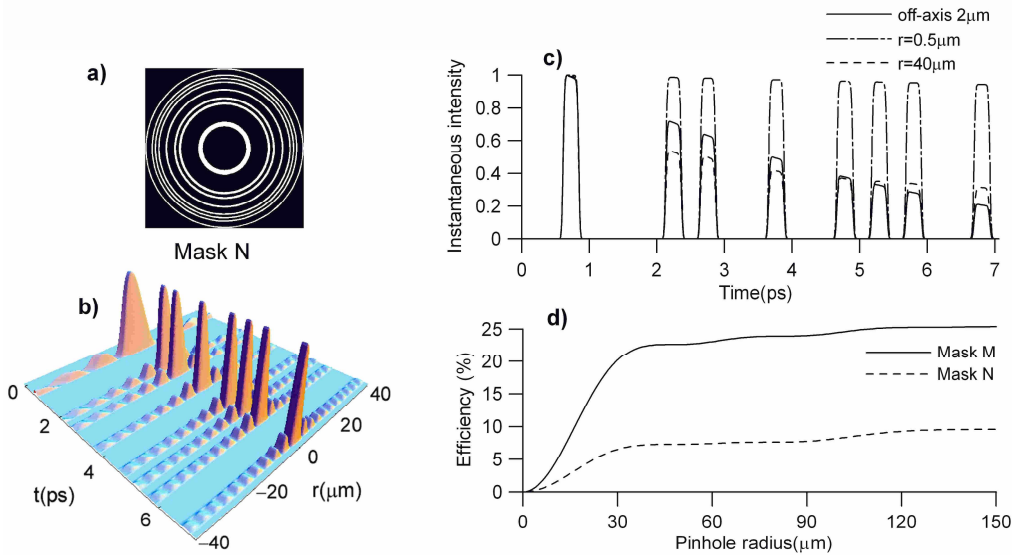

Fig. 3. (a). Mask N used for the generation of the binary code 01001101011101; (b) Normalized spatiotemporal intensity distribution for system in Fig. 1 by placing Mask N calculated for $z = 100$ mm; (c) Normalized output instantaneous intensity distribution for a punctual pinhole locate 2 μm off-axis (solid line) and for two on-axis pinholes of radii $r = 0.5$ μm (long-dashed line) and $r = 40$ μm (short-dashed line); (d) Monochromatic efficiency of the system as a function of the pinhole radius for masks M and N.

4. Conclusions

We present a novel QDST pulse shaper. The all-diffractive nature of the setup makes it suitable for working in different regions of the electromagnetic spectrum. This is especially useful when conventional lenses cannot be used, as with the XUV or X-ray radiation. The proposed technique utilizes the PTD associated with passage through a DL together with a circularly symmetric spatial mask to obtain the desired temporal amplitude. Computer simulations for the generation of a THz burst of pulses for telecommunication were shown.

Acknowledgments

This research was funded by the Spanish Ministry of Education and Science, Spain, and the Valencian Local Government Department of Trade, Universities and Science., under projects FIS2007-62217 and GV/2007/128, respectively. We acknowledge partial support from the Spanish Ministry of Education and Science through Consolider Program SAUUL CSD2007-00013. Omel Mendoza-Yero gratefully acknowledges financial support from the UJI-Fundació Caixa Castelló (Bancaixa) Agreement.

#98973 - $15.00 USD Received 18 Jul 2008; revised 22 Sep 2008; accepted 23 Sep 2008; published 10 Oct 2008